AIMS Materials Science, 9(4): 522–533.
DOI: 10.3934/matersci.2022031
Received: 11 February 2022
Revised: 13 April 2022
Accepted: 10 May 2022
Published: 30 June 2022

http://www.aimspress.com/journal/Materials

Research article

Pure TiO_2/PSi and TiO_2@Ag/PSi structures as controllable sensor for toxic gases

Ahmed Z. Abdullah, Adawiya J. Haider* and Allaa A. Jabbar

Department of Applied Sciences, University of Technology-Iraq, Baghdad, Iraq

* **Correspondence:** Email: adawiya.j.haider@uotechnology.edu.iq.

Abstract: In this research, two pellets of titanium dioxide TiO_2 were prepared at room temperature. The first was pure titanium dioxide, and the other was doped with silver (2.5%). The pellets were deposited on porous silicon (PSi) with the pulsed laser deposition (PLD) technique. The results of scanning electron microscopy and energy-dispersive X-ray spectroscopy showed improvements in the surface morphologies of the TiO_2/PSi and TiO_2@Ag/PSi composites. The composites were then tested as CO_2 gas sensors. The electrical measurements of the composites showed a decrease in the electrical resistance of the CO_2 gas sensor doped with a metal. Sensitivity to CO_2 increased to up to 55% in Ag-doped TiO_2 film with a concentration of 2.5%, and the highest sensitivity value was obtained in the pure titanium dioxide film (26%).

Keywords: porous silicon; photo-electrochemical etching; titanium oxide; pulsed laser deposition; sensitivity; gas sensor

1. Introduction

Porous silicon (PSi) has attracted considerable interest in recent years because of its unique physical and optical properties and many applications in technological fields, including optical electronics and sensors [1,2]. These characteristics are achieved by increasing its surface area in relation to its volume and the number of pores per unit volume [3]. Methods for producing PSi include the wet and galvanic methods and methods using metals. These methods are inexpensive, simple and efficient in preparing Psi [4,5]. PSi prepared with one of the etching methods shows new properties. The ordinary silicon, with an indirect energy gap of 1.12 eV, changes to PSi, with a direct

energy gap of 2.7 eV [6]. In the photo-electrochemical (PECE) method used in this study, an electrical cell with electrodes is used, and the negative electrode of platinum is connected to the negative part of an electric source. The anode is connected to the positive electrode of the electric current source. This electrode is made of silicon to be prepared as PSi. The cell is used as a container to contain a solution for photo-electrochemical reactions. The solution consists of fluoride acid at a concentration of 48%, which is diluted with HF:C_2H_5OH solution in a ratio of 1:1 [6,7]. When putting (100) n-type silicon wafer inside the container, it is connected to the anode, and this setup causes the wafer to be reverse biased, so a laser is used to generate an electron-hole pair on the wafer surface. The laser facilitates the passage of current in the cell, and then the reaction process begins. The photo-electrochemical technique is a suitable technique for preparing n-type PSi [8]. The porosity value of the PSi layer determines the application for which the PSi is used. For example, applications of optoelectronic and electronic sensors depend on the porosity [4,9]. PSi can be classified into three groups according to porosity: macrostructure, mesostructure and microstructure [1]. The porosity of the samples prepared by this technique (PECE) depends on several parameters, the most important of which are solution concentration, current density, etching time and laser beam intensity [2]. During the anodization of n-type Si, illumination is an essential control parameter that may be adjusted for the control of morphology (pore size, pore diameter and pore shape) and luminous characteristics [10,11]. PSi possesses the two most important properties that make it suitable for use as a gas sensor: a large internal surface area of up to 200–500 m^2/cm^2, which enhances adsorbate effects, and high activity in surface chemical reactions [12,13]. Metal oxides are commonly employed in the field of sensors due to their unique features [14–16]. Titanium dioxide thin film is used in gas sensors because of its desirable sensitivity and, more importantly, its excellent stability in adverse environments [17,18]. Silver with TiO_2 films is usually added to improve gas detector sensitivity [19–21].

2. Materials and methods

Figure 1 shows the conventional cell diagram required for photo-electrochemical etching, where n-type silicon with a crystalline direction of (100) is used, and the wafer is cut into pieces with 1 cm diameters and then cleaned with HF:C_2H_5OH solution in a ratio of 1:10. The samples were immersed in the solution and placed in an ultrasound device for 5 min, cleaned with distilled water and dried. Then, the samples were placed in the cell and linked, as shown in Figure 1. The greatest penetration depth of silicon was achieved using a laser with a long wavelength for the production of a thick layer of PSi. A 650 nm red color diode laser and an ammeter device were used in observing the amount of current passing through a sample and then determining current density during etching.

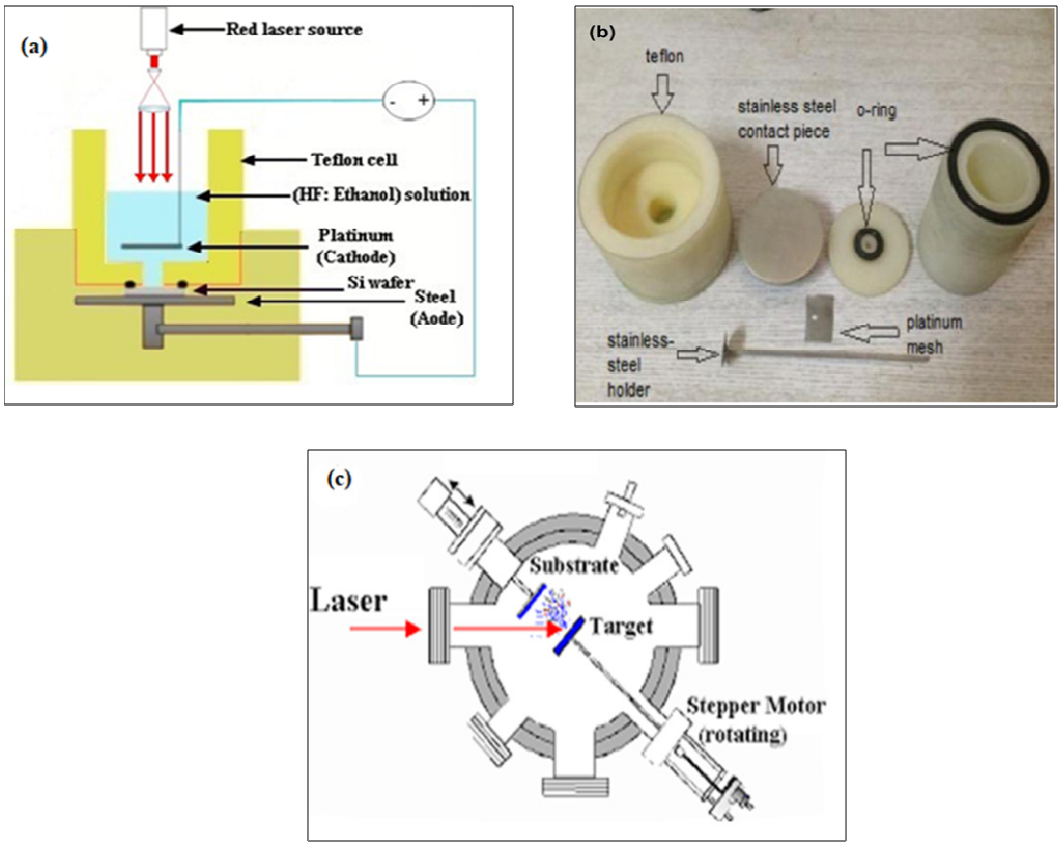

Figure 1. (a) Schematic drawing of a conventional single-tank etching cell, (b) photograph of the Teflon etching cell and (c) Pulsed laser deposition system scheme

Etching time was fixed at 15 min, and the intensity of the laser beam was set at 27 mW/cm^2. The current density was 16 mA/cm^2. After etching, the porosity was calculated for each sample according to the following weight equation [22,23]:

$$\text{Porosity\%} = \frac{w_1 - w_2}{w_1 - w_3} \tag{1}$$

where w_1 is the weight of the sample before the etching process, w_2 is the weight of the sample after etching, and w_3 is the weight of the sample after the removal of the porous layer with an NaOH solution. The solution was shaken for 20 min for the removal of the formed PSi. The thickness of the PSi layer was calculated using the equation below [22,23]:

$$\text{Thickness of PSi} = (w1 - w3)/(A_{PSi} \times d_{PSi}) \tag{2}$$

where A_{PSi} is the area of the PSi surface exposed to the HF acid solution through laser-assisted etching, and d_{PSi} is the silicon density.

After preparing the PSi samples, the thin film is prepared according to the application. Figure 1c shows the PLD system used in deposition. The system consisted of a chamber containing a holder where a sample to be deposited would be placed and a rotating bench where the target material would be placed. Increase in temperature in a specific area was prevented by rotating the target. The chamber was emptied of air until the pressure reached 10^{-1}–10^{-3} bar. We deposited titanium dioxide

on some of the prepared samples with the PLD technique [24,25]. A helium-neon laser with a wavelength of 532 nm (second harmonic) and energy of 0.8–1.8 mJ/cm^2 was used at a frequency of 3 Hz and laser pulse of about 100 pulses. TiO_2 powder was used and prepared in the form of a compact disc (pellet) with a diameter of 2.1 cm and a weight of 3 g. The disc was placed under a pressure of 10 tons for 5 min and then inserted into the chamber, which in turn was placed on an electric motor that rotated continuously. The prepared samples deposited with titanium dioxide were placed against the target material (disc), and the chamber was emptied of air until the pressure reached 10^{-3} bar.

An external laser was used to bombard the target material at an angle of 45º. The substance was melted, converted into plasma and detonated. The process resulted in the deposition of atoms and volatile particles on the PSi. After deposition, the samples were heated at 300 ℃ for 15 min using a helium-neon laser with an energy range of 0.8–1.8 mJ, frequency of 3 Hz and wavelength of 532 nm (second harmonic). The surface was examined through scanning electron microscopy (SEM) and energy dispersive X-ray spectroscopy (EDS), and the electrodes were deposited on the pure and doped TiO_2/PSi surfaces.

3. Results and discussion

3.1. PSi surface morphology

3.1.1. Bare PSi surface morphology

Figure 2 displays the SEM images of the fabricated PSi surface with a 15 min etching time, fixed laser beam intensity of 27 mW/cm^2 and current density of 16 mA/cm^2.

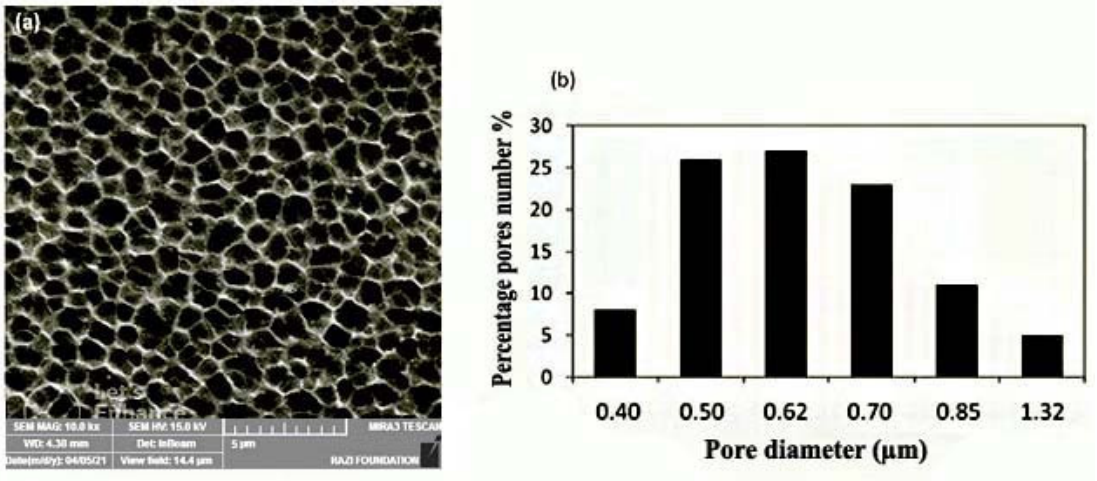

Figure 2. SEM images of (a) bare PSi layer and (b) statistical distribution.

The surface of the PSi presented a pore-like structure, and the pores were randomly distributed in the form of tetragonal cylindrical, pentagonal and hexagonal pores. The distribution of the pores was somewhat homogeneous [26]. Table 1 shows that the pore diameters ranged from 0.40 to 1.32 µm, and the peak distribution was about 0.62 µm. The percentage of pores was 27%, and the porosity

value and layer thickness were 62% and 4.2 μm, respectively (the values were calculated using Eqs 1 and 2, respectively). The porosity of the PSi layer was determined by the etching current density used in the photo-electrochemical etching process, whereas the thickness of the PSi layer was determined by the etching time [5,27,28].

Table 1. Profile of PSi layer.

Porosity of PSi layer	Psi layer thickness (μm)	Percentage pores number (%)	Range of pore diameters (μ)
62	4.2	26–27	0.50–0.62

3.1.2. PSi surface morphology after deposition

The PSi surface was studied using the two different deposition compounds of pure TiO_2 and silver-doped TiO_2 at a concentration of 2.5%. The deposition of the compounds was carried out with the PLD technique and a helium-neon laser (second harmonic) with a wavelength of 532 nm. Laser energy and frequency were 1.8 mJ and 3 Hz, respectively.

As indicated in Figure 3a, the statistical distribution indicated that the isolated TiO_2 nanoparticles (NPs) were spread heterogeneously over the PSi surface, and the particle diameters ranged from 7 to 225 nm. The peak size was around 90 nm. The statistical distribution indicated that the TiO_2@Ag NPs were spread homogenously over the PSi surface, the particle diameters ranged from 38 to 222 nm, and the peak size was around 38 nm. The doping of titanium oxide with silver exerted an effect on the surface area value, particle size, energy gap and photocatalytic activity [29]. Gas sensor sensitivity is a function of particle size, surface morphology, crystal structure, and conditions of preparation [17,30,31].

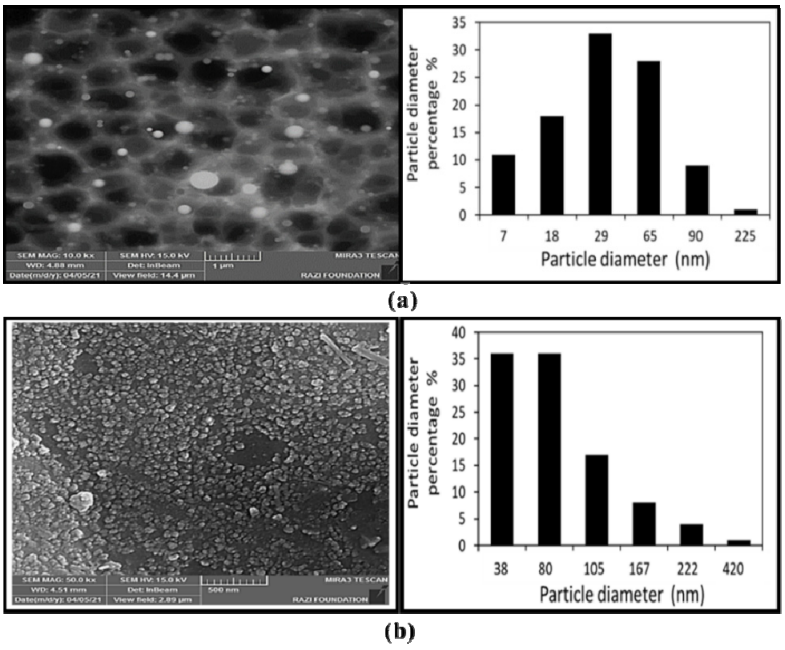

Figure 3. SEM images and the statistical distributions of (a) PSi layer after deposit with pure TiO_2 and (b) PSi layer after deposit with TiO_2 doped by Ag.

3.2. Energy-dispersive X-ray spectroscopy (EDS) analysis

The EDS result in Figure 4a shows a high Si content (42.76%) and moderate Ti content (6.25%). The high percentage of the O element (49.22%) was due to the amounts of the O element in the silicon oxide layer and TiO_2.

Figure 4b shows the presence of Ag element with a content of 0.92% in the TiO_2@Ag (2.5%)/PSi sample with a large content of Ti (29.25%). The appearance of the carbon element may be due to the components of the solvents used in photo-electrochemical etching.

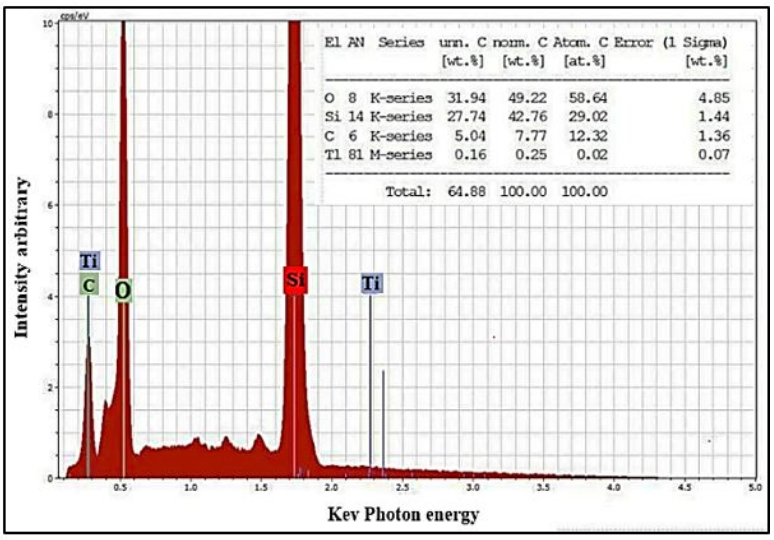

(a)

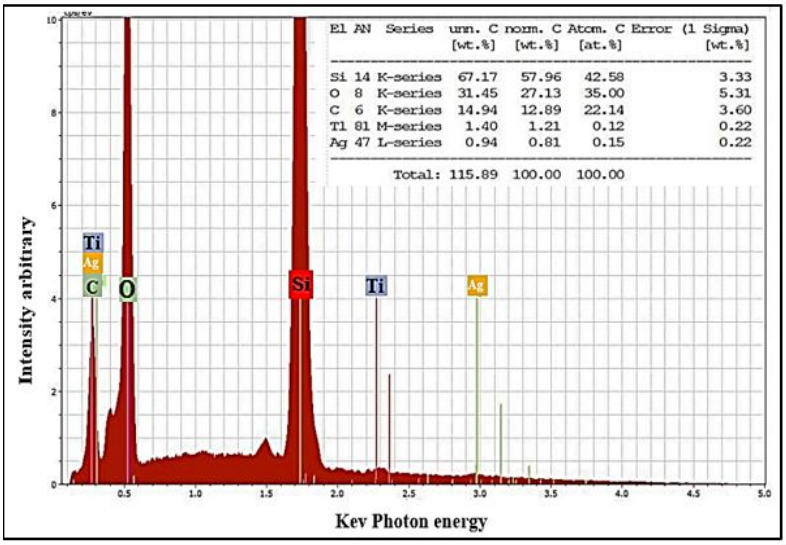

(b)

Figure 4. EDS analysis of (a) PSi layer after deposition with pure TiO_2 and (b) PSi layer after deposition with TiO_2 doped by Ag.

3.3. X-ray diffraction (XRD)

The XRD examination was carried out to characterize the crystal structure type and the crystalline size of the prepared samples. Figure 5 presents the XRD patterns of the TiO_2 nanoparticles on PSi and the Ag doped TiO_2 thin film (Ag 2.5 wt%) on PSi. The detected characteristic peaks of TiO_2/PSi at (2θ = 27.5°), (2θ = 36.14°), (2θ = 39.28°), (2θ = 41.34°), (2θ = 54.44°) and (2θ = 56.79º) of the planes (110), (101), (200), (111), (211) and (220) indicated the formation of tetragonal TiO_2 (Rutile) nanoparticles with space group (P42/mnm no. 136), dimensions (a = b = 4.582 Å, c = 2.953 Å) and angles (α = β = γ = 90°), which agreed well with the standard data (JCPDS 065-0192). In addition, a strong peak appeared at (2θ = 69.02°) of the plane (004), which is attributed to the PSi layer.

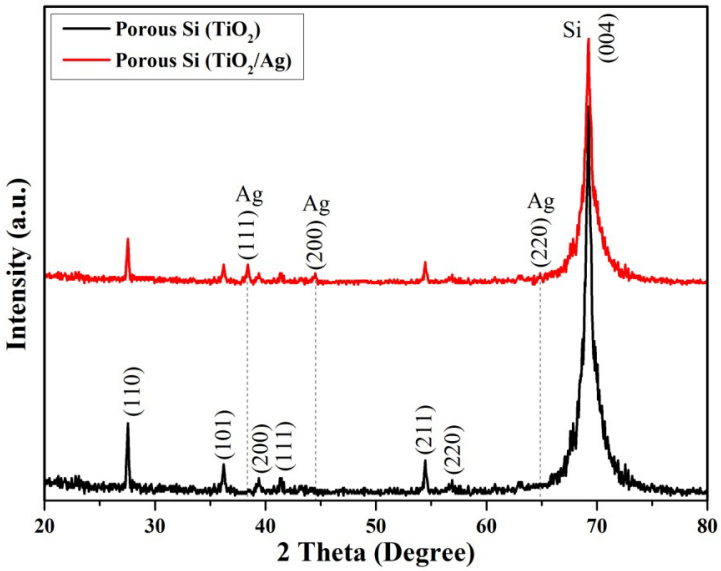

Figure 5. XRD patterns of (a) PSi layer after deposition with pure TiO_2 and (b) PSi layer after deposition with TiO_2 doped by Ag (2.5%).

After doping with silver (TiO_2@Ag/PSi), three new peaks appeared at (2θ = 38.28°), (2θ = 44.47°) and (2θ = 64.72°) of the planes (111), (200) and (220), which were attributed to the cubic silver nanoparticles with space group (Fm-3m no. 225), dimensions (a = b = c = 4.071 Å) and angles (α = β = γ = 90°), which corresponded to the standard data (JCPDS 087-0719). The peaks' intensities decreased with the addition of silver in the structure of the TiO_2/PSi, and no other impurities' peaks were detected, indicating the high purity phases of the prepared TiO_2/PSi and (TiO_2@Ag/PSi) samples.

3.4. Electrical properties of TiO_2/PSi and TiO_2@Ag (2.5%)/PSi sensors with CO_2 gas

The electrical properties of the prepared samples were measured, including electrical resistance and sensitivity, as these properties depend mainly on preparation conditions, film thickness and percentage of impurities within a membrane material.

3.4.1. Resistance-time characteristics of pure TiO_2/PSi and TiO_2@Ag (2.5%)/PSi sensors with CO_2 gas

As shown in Figure 6, the electrical resistances of the samples with pure TiO_2/PSi and $TiO_{2@}$Ag/PSi sensors were measured. The conductivity of the TiO_2/PSi sensor became considerably higher than that of the pure TiO_2 film. The general behavior of the gas sensor was to increase in resistance after exposure to the gas. In the pure TiO_2/PSi sensor, the gas received charge carriers from the titanium oxide/PSi substrate. The gas oxidized titanium oxide, so the sensor resistance increased.

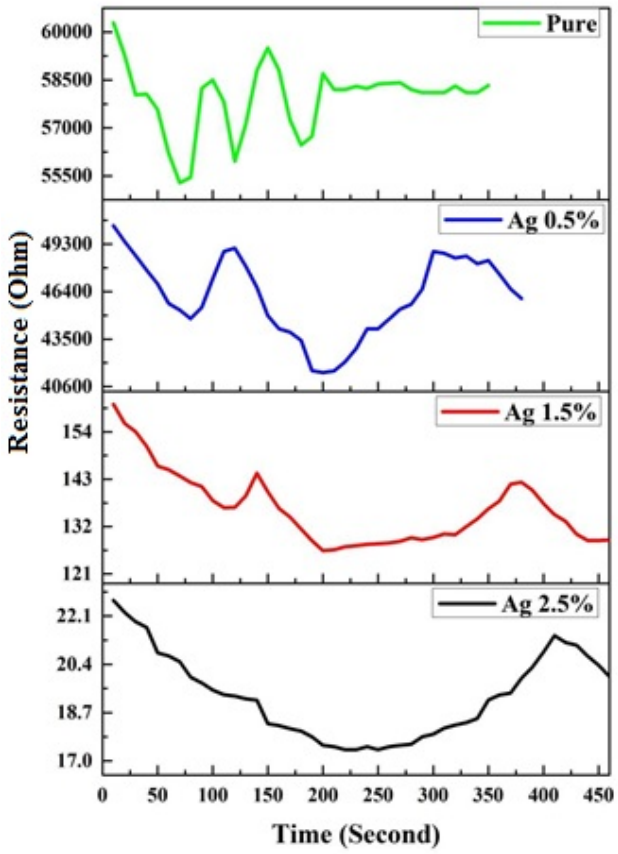

Figure 6. Electrical resistance vs. time (for 5000 ppm CO_2 gas) of PSi layer deposited with pure TiO_2 and PSi layers deposited with TiO_2 doped by Ag at different concentrations.

As shown in Figure 6, in doping with silver ($TiO_{2@}$Ag/PSi sensor, Ag 2.5%), metal ion dopants affected TiO_2 by acting as electron (or hole) traps and modifying the e-/h+ pair recombination rate in addition to reducing the transition energy of electrons. In doping with silver (TiO_2@Ag/PSi sensor), the same gas that was exposed to the sensor transformed from an oxidizing gas to a reducing gas, that is, it provided electrons to the substrate after doping with silver. The presence of silver resulted in increased electrical conductivity, which in turn caused a drop in sensor resistance. The gas in the presence of silver metal turned from an electron-withdrawing gas to an electron-donating gas [32,33],

so the electrical conductivity increased, and the resistance decreased. This finding was consistent with results from other sources [17,34,35].

3.4.2. Sensitivity of pure TiO_2/PSi and TiO_2@Ag/PSi sensors in the presence of CO_2 gas

The interaction between the target gas molecules and the sensor surface determined the sensitivity of the metal oxide semiconductor sensor. The gas-detecting sensitivity of the sensor increased with the surface areas of the materials and strengths of the interactions between the adsorbed gases and the sensor surface. TiO_2 doped with Ag metal had a higher sensitivity to CO_2 gas, as shown in Figure 7. Given that surface species and trapped electrons were restored to the conduction band, TiO_2 films doped with noble metals exhibited increased conductivity and thus increased sensitivity. The majority of the gas-sensitive structures were n-type semiconductors, owing to intrinsic doping provided by the preparation methodologies, and thus p-type semiconductors sensitive to gases were lacking. P-type semiconductor gas sensors showed gas-sensing patterns different from those of n-type ones. TiO_2-doped Ag has been considered a p-type gas sensor. Notable differences between n-type and p-type Ag-doped TiO_2 were found, and p-type Ag doping resulted in significant response enhancement toward tested reducing gases.

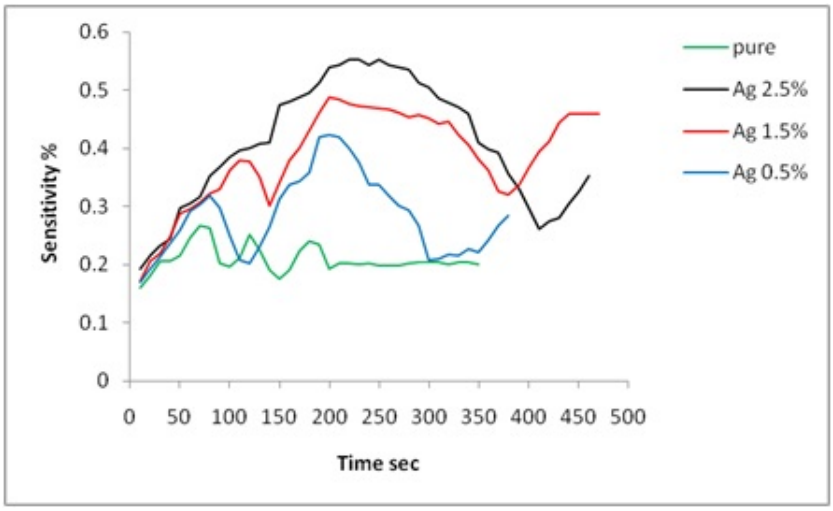

Figure 7. Sensitivity vs. time (for 5000 ppm CO_2 gas) of PSi layer after deposition with pure TiO_2 and PSi layers after deposition with TiO_2 doped by Ag with different concentrations (0.5%, 1.5% and 2.5%).

4. Conclusions

In this study, two types of gas sensors were manufactured. The first was pure titanium oxide particles deposited (by PLD) on a PSi layer, and the other was mixed silver (2.5%) and titanium oxide deposited on the same PSi layer. The performance of the gas sensors improved with the mixing of titanium oxide with silver and the deposition of titanium oxide on the surface of the PSi. The surface morphology of the surface facilitated the capturing of gas particles by increasing the surface area and the determination of the shape and size of deposited silver and titanium oxide particles.

Moreover, the addition of silver with titanium contributed to the reduction of the resistance of the sensor and increased its sensitivity after a gas exposed to the sensor was transformed from an oxidizing gas to an ionized gas.

Acknowledgments

The authors gratefully acknowledge the financial and technical support provided by the Applied Sciences Department, University of Technology- Iraq, Baghdad, Iraq.

Conflicts of Interest

The authors declare no conflict of interest.

References

1. Korotcenkov G (2016) Optoelectronics, microelectronics, and energy technology applications, *Porous Silicon: From Formation to Applications*, CRC Press.
2. Canham LT (1997) *Properties of Porous Silicon*, London: Inst of Engineering & Technology.
3. Haider AJ (2008) The effect of some experimental parameters on the properties of porous silicon. *IJAP* 4: 37–40.
4. Haider AJ, Al-Anbari R, Sami HM, et al. (2019) Enhance preparation and characterization of nickel-oxide as self-cleaning surfaces. *Energ Procedia* 157: 1328–1342. https://doi.org/10.1016/j.egypro.2018.11.298
5. Parkhutik V (1999) Porous silicon-mechanisms of growth and applications. *Solid State Electron* 43: 1121–1141. https://doi.org/10.1016/S0038-1101(99)00036-2
6. Jabbar AA, Haider AJ, Haider MJ, et al. (2020) Preparation and characterization of NiO/PSi as self-cleaning surface. *J Mater Res Technol* 9: 15123–15131. https://doi.org/10.1016/j.jmrt.2020.10.075
7. Sailor MJ (2012) *Porous Silicon in Practice: Preparation, Characterization and Applications*, John Wiley & Sons. https://doi.org/10.1002/9783527641901
8. Goryachev D, Belyakov L, Sreseli O (2003) Electrolytic fabrication of porous silicon with the use of internal current source. *Semiconductors* 37: 477–481. https://doi.org/10.1134/1.1568472
9. Lang W (1996) Silicon microstructuring technology. *Mater Sci Eng R* 17: 1–55. https://doi.org/10.1016/0927-796X(96)00190-8
10. Bomchil G, Halimaoui A, Herino R (1988) Porous silicon: the material and its applications to SOI technologies. *Microelectron Eng* 8: 293–310. https://doi.org/10.1016/0167-9317(88)90022-6
11. Bisi O, Ossicini S, Pavesi L (2000) Porous silicon: a quantum sponge structure for silicon based optoelectronics. *Surf Sci Rep* 38: 1–126. https://doi.org/10.1016/S0167-5729(99)00012-6
12. AA Salih, AJ Haider, A Nazar (2020) Preparation and characterizations of nanomaterial by pulsed laser ablation in liquid (PLAIL) as friendly environment paint. *J Phys Conf Ser* 1795: 012023. https://doi.org/10.1088/1742-6596/1795/1/012023
13. Ozdemir S, Gole JL (2007) The potential of porous silicon gas sensors. *Curr Opin Solid St M* 11: 92–100. https://doi.org/10.1016/j.cossms.2008.06.003

14. Carpenter MA, Mathur S, Kolmakov A (2012) *Metal Oxide Nanomaterials for Chemical Sensors*, Springer Science & Business Media. https://doi.org/10.1007/978-1-4614-5395-6
15. Manjakkal L, Szwagierczak D, Dahiya R (2020) Metal oxides based electrochemical pH sensors: Current progress and future perspectives. *Prog Mater Sci* 109: 100635. https://doi.org/10.1016/j.pmatsci.2019.100635
16. Saleh AA, Haider AJ, Nazar A (2021) Preparation and properties of mattel oxide nanoparticles by pulse laser ablation in liquid as photo-catalysis. *Key Eng Mater* 900: 197–204. https://doi.org/10.4028/www.scientific.net/KEM.900.197
17. Abed AL, Mohammed FQ, Hasan AS (2017) Synthesis and study of modified nanostructure porous silicon layers for chemical gas sensing. *Eng Technol J* 35: 970–974.
18. Kahdim GR, AL-Anbari RH, Haider AJ (2018) Preparation and characterization of TiO_2 nanoparticles and its applications as antibacterial agents. *Eng Technol J* 36: 1068–1074. https://doi.org/10.30684/etj.36.10A.7
19. Navale S, Shahbaz M, Mirzaei A, et al. (2021) Effect of Ag addition on the gas-sensing properties of nanostructured resistive-based gas sensors: An overview. *Sensors* 21: 6454. https://doi.org/10.3390/s21196454
20. El-Sayet A, Ismail F, Yakout S (2011) Electrical conductivity and sensitive characteristics of Ag-added $BaTiO_3$-CuO mixed oxide for CO_2 gas sensing. *J Mater Sci Technol* 27: 35–40. https://doi.org/10.1016/S1005-0302(11)60022-4
21. Alwan AM (2014) An investigation of multi-porous silicon gas sensor. *Eng Technol J* 32: 183–190.
22. Basu S (2011) *Crystalline Silicon: Properties and Uses*, BoD-Books on Demand. https://doi.org/10.5772/844
23. Hwang J, Hwang S, Chou C, et al. (2011) Investigation of opto-electronic properties on gradient-porosity porous silicon layer. *Thin Solid Films* 519: 2313–2316. https://doi.org/10.1016/j.tsf.2010.11.041
24. Haider AJ, Jabbar AA, Ali GA (2021) A review of pure and doped ZnO nanostructure production and its optical properties using pulsed laser deposition technique. *J Phys Conf Ser* 1795: 012015. https://doi.org/10.1088/1742-6596/1795/1/012015
25. Haider AJ, Al-Kinani MA, Al-Musawi S (2021) Preparation and characterization of gold coated super paramagnetic iron nanoparticle using pulsed laser ablation in liquid method. *Key Eng Mater* 886: 77–85. https://doi.org/10.4028/www.scientific.net/KEM.886.77
26. Carlsson JM (2010) Simulations of the structural and chemical properties of nanoporous carbon, In: Colombo L, Fasolino A, *Computer-Based Modeling of Novel Carbon Systems and Their Properties*, Springer, 79–128. https://doi.org/10.1007/978-1-4020-9718-8_4
27. Hadi HA, Ismail RA, Habubi NF (2013) Fabrication and characterization of porous silicon layer prepared by photo-electrochemical etching in CH_3OH: HF solution. *ILCPA* 3: 29–36. https://doi.org/10.18052/www.scipress.com/ILCPA.8.29
28. Maniya NH, Patel SR, Murthy Z (2013) Electrochemical preparation of microstructured porous silicon layers for drug delivery applications. *Superlattice Microst* 55: 144–150. https://doi.org/10.1016/j.spmi.2012.12.005
29. Mogal SI, Mishra M, Gandhi VG, et al. (2013) Metal doped titanium dioxide: synthesis and effect of metal ions on physico-chemical and photocatalytic properties. *Mater Sci Forum* 734: 364–378. https://doi.org/10.4028/www.scientific.net/MSF.734.364

30. Korotcenkov G (2013) Conventional approaches, *Handbook of Gas Sensor Materials*, Springer. https://doi.org/10.1007/978-1-4614-7165-3
31. Mariappan R, Ponnuswamy V, Suresh P, et al. (2014) Influence of film thickness on the properties of sprayed ZnO thin films for gas sensor applications. *Superlattice Microst* 71: 238–249. https://doi.org/10.1016/j.spmi.2014.03.029
32. Faburada AL (1978) *The Effects of Electron-donating and Electron-with Drawing Groups on the Alkylation Sites of Para-substituted Phenylacetones*, Western Michigan University ProQuest Dissertations Publishing.
33. Haider AJ, Mutasher HA (2015) A study on the structural, optical and electrical properties of tungsten trioxideWO3 thin film for gas sensing applications. *Eng Technol J* 33: 1473–1482.
34. Sheini NA, Rohani M (2016) Ag-doped titanium dioxide gas sensor. *IOP Conf Ser Mater Sci Eng* 108: 012033. https://doi.org/10.1088/1757-899X/108/1/012033
35. Ramesan M, Santhi V, Bahuleyan B, et al. (2018) Structural characterization, material properties and sensor application study of in situ polymerized polypyrrole/silver doped titanium dioxide nanocomposites. *Mater Chem Phys* 211: 343–354. https://doi.org/10.1016/j.matchemphys.2018.02.040

AIMS Press